Mechanical Behavior of Tailings Sands: A Numerical Analysis using the UBCSAND Constitutive Model

Reynaldo Melquiades Reyes Roque
Academic Professional School of Civil Engineering, Faculty of Civil Engineering, National University of Santiago Antunez Mayolo, Huaraz, 02002, Ancash, Peru
rreyesr@unasam.edu.pe (corresponding author)

Gianina Mariela Chinchay Poma
Academic Professional School of Civil Engineering, Faculty of Civil Engineering, National University of Santiago Antunez Mayolo, Huaraz, 02002, Ancash, Peru
gianina.chinchay@unmsm.edu.pe

Hirbin Felix Cespedes Reynaga
Department of Civil Engineering, Faculty of Science and Engineering, Pontificia Universidad Catolica del Peru, 15088, Lima, Peru
hcespedes@pucp.edu.pe

Ronald Madera Teran
Professional School of Civil Engineering, Faculty of Engineering and Pure Sciences, Universidad Andina Nestor Caceres Velasquez, 211101, Juliaca, Peru
d02429150@uancv.edu.pe

Santiago Alberto Casas Luna
School of Health Engineering, Faculty of Ecology, Universidad Nacional de San Martin, 22200, Tarapoto, Peru
scasasl@unsm.edu.pe

Received: 29 January 2025 | Revised: 14 March 2025 | Accepted: 22 March 2025

 DOI: https://doi.org/10.48084/etasr.10380

ABSTRACT

This study aimed to demonstrate the practical advantages of the UBCSAND constitutive model in simulating the mechanical behavior of tailings sands through numerical analysis. For this purpose, a mixed approach of non-experimental design, applied type, and comparative scope was chosen. The population consisted of 20 monotonic triaxial tests for tailings sands and the purposive sample consisted of 3 tests performed with confining stresses of 5, 10, and 15 kg/cm^2 under undrained conditions. Simulations were performed using the TNO DIANA finite element software, which incorporates the UBCSAND model. The validation of the model's implementation was achieved by comparing its predictions with both the experimental results and simulations conducted using the PLAXIS program. The results indicated that the numerical responses of stress-strain, volumetric change-strain, and stress path, showed a strong compatibility with the experimental data at a confining stress of 5 kg/m^2, while for higher values (10 and 15 kg/m^2) there was still a good agreement with some moderate observations. Consequently, the study proposes that the UBCSAND constitutive model is an efficient alternative approach to predict with high accuracy the mechanical behavior of tailings sands.

Keywords-constitutive model; mechanical behavior; numerical analysis; UBCSAND model; monotonic triaxial test

I. INTRODUCTION

The identification of soil types is a crucial step in the evaluation and execution of engineering activities [1]. The importance of geotechnical engineering for analysis, design, and implementation is pronounced during project development on vast scales [2]. This highlights that soil characterization is equally important for project cost-benefit analysis apart from structural arrangements [3]. Several studies have investigated the mechanical behavior of tailings sands. For example, in [4] author highlighted that current engineering practices rely on in situ measurements and simplified procedures, which do not consider the cross interaction between the different layers during the liquefaction process, specifically the water flow and pore pressure dissipation. In [5], the drained cyclic response of tailings sands based on the critical state theory was investigated, with the results revealing that settlements occur only when the current seismic load exceeds any previous seismic event. Additionally, a strong correlation between settlement, cyclic shear stress, and the critical-state parameter (ψ_0) was observed.

Authors in [6], analyzed the liquefaction susceptibility of silty tailings using monotonic triaxial tests under semi-saturated conditions. The results were compared with literature data to evaluate the dependence on the preparation method, volumetric water content, void ratio, and degree of saturation. This analysis indicated that the static liquefaction response depended mainly on the preparation technique and the degree of saturation. The latter, in turn, controls the excess pore pressure, whose leading role was examined through the relationship between Skempton's parameter *B* and the degree of saturation. From the same perspective, authors in [7] pointed out that the particle size distribution of tailings sands influences their strength, deformation, and mechanical properties, further affecting overall safety and stability. Through undrained consolidation tests on five particle size groups, they concluded that the larger the particle is, the higher is the shear strength. By changing the sample gradation, the coefficient of uniformity (*Cu*) and coefficient of curvature (*Cc*) remained constant, while by adjusting another parameter, a close relationship was observed between *Cu*, *Cc,* and the shear strength. Furthermore, authors in [8, 9] agreed that the soil's behavior under different loads needs extensive analysis. Numerical analysis, using triaxial tests is essential for assessing the mechanical strength of sandy soils in geotechnical engineering. This computational approach enables more precise evaluation of strength characteristics under monotonic loading conditions. Authors in [8, 10] confirm that triaxial testing is a validated technique for measuring the shear strength of sand. These tests reproduce, in an approximate manner, the in situ conditions subjected to confining stresses. In [11-13], it was stated that in order to efficiently manage the laboratory data, constitutive models are required. In these models, sand is considered a continuous medium, whose constitutive equations represent stress-strain relationships with advanced mathematical formulations. In this line of research, authors in [14, 15] revealed that these models include mathematical formulations capable of describing the macroscopic physical behavior of an ideal solid, derived from the application of simplifying assumptions on a real material. A relevant study, [16], evaluated the behavior of an iron ore tailing of the Ferriferous Quadrangle using critical state computational models (Modified Cam-Clay and NorSand). It was observed that, in loose samples, both models produced similar results. Based on [16], the present work focuses on determining the applicational advantages of an alternative model, defined as UBCSAND model, on the mechanical behavior of tailings sands. To achieve this, a non-experimental, applied, mixed-method approach with a descriptive-comparative scope was adopted [17-19]. The study population consisted of 20 records of monotonic triaxial tests with tailings sands from the El Torito dam, located at the El Soldado copper mine in Santiago, Chile, with a relative density of 40%. Also, the sample included three monotonic triaxial tests performed under undrained conditions. These tests were recorded following the methodology applied in [7], under confining stresses of 5, 10, and 15 kg/cm^2, respecting the principle of non-probabilistic purposive sampling [20].

II. THE UBCSAND CONSTITUTIVE MODEL

In recent years, constitutive models are responsible for solving various geotechnical problems, even in highly complex scenarios. Their application guarantees the accuracy of laboratory data, by facilitating the simulation of material behavior through relating variables, such as stress and strain, while considering the specific mechanical properties of the material under study [21]. Among the various models developed, the UBCSAND model, as mentioned in [22], stands out. This model is a simple elastoplastic stress-strain formulation designed to simulate the liquefaction phenomena in sand, especially for materials with a relative density below 80%.

For its application, it is assumed that the elastic response is isotropic, and is governed by the shear modulus (G^e) and the bulk modulus B^e:

$$G^e = K_G^e \times P_a \times \left(\frac{\sigma'}{P_a}\right)^{n_e} \quad (1)$$

$$B^e = K_B^e \times P_a \times \left(\frac{\sigma'}{P_a}\right)^{m_e} \quad (2)$$

where K_G^e is the elastic shear modulus number, which can be associated with SPT-N values, P_a is the atmospheric pressure, σ' is the mean effective stress in the loading plane, n_e is the exponent variable that relates the elastic shear modulus to the mean effective stress, K_B^e is the bulk elastic modulus number, which depends on Poisson's ratio, and m_e is the elastic exponent variable that relates the bulk modulus to the mean effective stress.

The plastic response of the material is divided into shear plastic strain (γ^p) and volumetric plastic strain (ε_v^p), controlled by a yield surface and a flow rule. The yield surface is defined as a radial line from the origin in the $\sigma' - \tau$ (mean effective stress-shear strain space). As the shear stress ratio ($\eta = \frac{\tau}{\sigma'}$) changes, the increase in shear plastic strain ($d\gamma^p$) is governed by:

$$d\gamma^p = \left(\frac{\sigma'}{G^p}\right) \times d\eta \quad (3)$$

$$G^p = G_i^p \times \left(1 - \left(\frac{\eta}{\eta_f} \times R_f\right)^2\right) \quad (4)$$

$$G_i^p = K_G^p \times P_a \times \left(\frac{\sigma'}{P_a}\right)^{n_p} \quad (5)$$

where G^p is the plastic shear modulus, $d\eta$ is the increment of the stress ratio, G_i^p is the plastic shear modulus at a low shear stress ratio level, $\eta_f = sin\phi_{peak}$ is the failure stress ratio, ϕ_{peak} is the peak friction angle, R_f is the failure ratio, K_G^p is the plastic shear modulus number, and n_p is an exponential variable that relates the plastic shear modulus to the mean effective stress.

As a derivation, a non-associated flow rule is adopted to connect the increase of plastic volumetric deformation ($d\varepsilon_v^p$) with the increase of plastic shear deformation ($d\gamma^p$), according to the following expression:

$$d\varepsilon_v^p = (sin\phi_{cv} - \frac{\tau}{\sigma'}) \times d\gamma^p \quad (6)$$

where ϕ_{cv} is the constant volume friction angle or phase transformation angle.

When the shear stress ratio η is equal to $\sin(\phi_{cv})$, the increase in plastic volumetric strain is zero and the material is in a constant volume condition. Otherwise:

- If $\eta > \sin\phi_{cv}$, $d\varepsilon_v^p$ is negative and the material is in a dilatant condition.
- If $\eta > \sin\phi_{cv}$, $d\varepsilon_v^p$ is positive and the material is in a shrinkage condition.

From an applicative approach, this model has been integrated into the TNO DIANA software platform as a part of a numerical modeling scheme based on monotonic triaxial test results [23] under both drained and undrained conditions [24, 25]. The TNO DIANA initiative is a multipurpose finite element code program designed to address a wide variety of problems in civil engineering, including structural, geotechnical, tunneling, and seismic engineering, as well as applications in the oil and gas industry [26, 27]. It is important to consider that, in order to develop specific tests in this software, a number of input parameters are required, as specified.

Regarding the application and use of the studied model, authors in [28] carried out a comparative analysis between the predictions of the UBCSAND and the Hypoplastic Soil (HPS) model. They employed the Material Point Method (MPM) and implemented the Convective Particle Domain Interpolation (CPDI), an advanced technique of MPM, for dynamic loading simulations. The UBCSAND model was calibrated with Berlin sand and its numerical predictions were compared with experimental data to evaluate its performance. A shaking table test was simulated in the laboratories of the Rensselaer Polytechnic Institute. These findings exhibited excellent agreement with the experiments and numerical calculations. Both models were further tested by simulating a driven pile installation. It was verified that the multiphase CPDI formulation reproduces the liquefaction phenomenon in the case of pile driving. Additionally, in [29], the results of cyclic and monotonic drained compression tests on four types of aggregates were evaluated as well as the applicability of the UBCSAND model to represent nonlinear stress-strain curves. The model was analytically integrated for both volumetric and deviatoric deformations, elastic and plastic, leading to new closed-form solutions expressed by hypergeometric functions. These solutions eliminated numerical errors and facilitated the interpretation of the results. Subsequently, the authors presented and compared three calibration techniques for parameter calibration:

- Graphical solution based on direct numerical simulations,
- A numerical approach based on residual minimization,
- A trial-and-error method based on the analytical solution.

Then, they examined the errors of numerical integration of the model by comparing the analytical solution against the results obtained by Euler integration. The authors analyzed variations of the calibrated parameters under cyclic and monotonic drained triaxial loading using different kinds of aggregates. They concluded that model parameters calibrated under monotonic conditions are not always able to predict accurately during cyclic loading, especially for cycles longer than 1-4. Therefore, UBCSAND needs to be calibrated according to the particular conditions so that the mechanical response corresponding to specific loading situations can be captured appropriately. Another important study is [30], where the seismic deformation of earth dams subject to liquefaction was explored using the UBCSAND2 model. Their findings indicated that this model allowed the incorporation of the initial horizontal stress ratio $K = \frac{\sigma'_x}{\sigma'_y}$ in simulating soil elements on slopes under direct simple shear conditions. This stress factor is generally neglected in liquefaction predictions when using alternative practical constitutive models.

The initial calibration for the UBCSAND2 model considered the typical drained and undrained behaviors of individual elements subjected to both monotonic and cyclic Direct Simple Shear (DSS) loading, using generic input parameters for various relative densities. The model was then fitted using empirical data obtained from liquefaction activation weighting curves. The results demonstrated that the development of the fault shear band on the upstream side was consistent with observed post-liquefaction slip surfaces.

III. DETERMINATION OF INPUT PARAMETERS FOR THE UBCSAND MODEL IN TNO DIANA SOFTWARE

To validate the application of the UBCSAND model within the TNO DIANA software, an eight-node brick-type volume finite element with unit dimensions along the X, Y, and Z axes was developed. This approach follows the methodology described in [31].

The TNO DIANA program [32] provides a graphical interface that enables rapid generation of finite element meshes, definition of boundary conditions, and application of different loading stresses. The load application is performed in two well-defined stages. Similar to the triaxial test, the numerical analysis procedure consisted of confining and deviatoric stresses. In the first stage, the confining stress

simulation considers normal stresses with equal values $\sigma_1 = \sigma_3$, which represent an isotropic confining stress characteristic of the triaxial test. This load is applied on three faces of the element in the XZ, YZ, and XY planes. In the second stage, vertical deformations are imposed on the top face of the cubic element to simulate the application of the deviatoric stress $q = \sigma_1 - \sigma_3$.

Figures 1 and 2 indicate that the UBCSAND model has been correctly validated in TNO DIANA software. This confirmation was performed based on the study in [33], regarding the UBCSAND model implemented in PLAXIS.

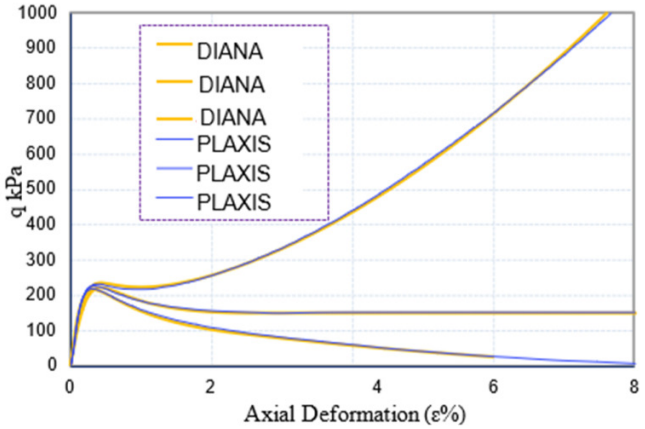

Fig. 1. Validation of the UBCS and model implemented in the TNO Diana program in relation to the one presented by PLAXIS for the axial stress-strain curve.

Undrained simulations of expansive, contractive, and highly contractive samples have been adequately represented. In highly contractive samples, as depicted in Figure 1, the critical state friction angle was slightly lower than the friction angle at constant volume. In contractive samples, both angles tended to coincide, whereas, in expansive behavior, the critical state friction angle exceeded the friction angle at constant volume. Table I illustrates this relationship more clearly. As for the strength, in the highly contractive samples, as portrayed in Figure 2, it is observed that the sand loses its strength as the load increases until a zero value is reached, a response characteristic of static liquefaction.

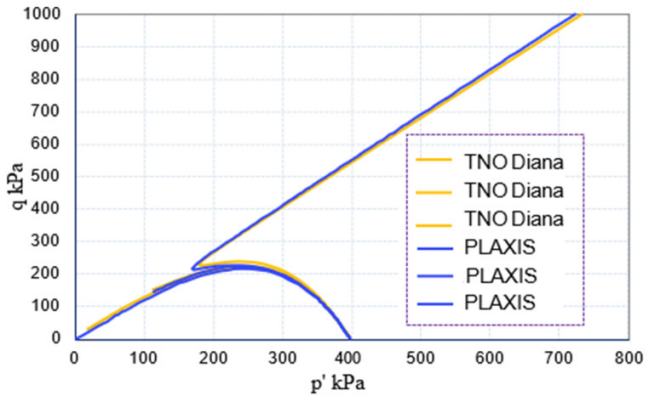

Fig. 2. Validation of the UBCS and model implemented in the TNO Diana program in relation to the one presented by PLAXIS for the trajectory of effective efforts.

In the sample that undergoes phase transformation, the initial response to shear is contractive, with a similar behavior being represented in both TNO DIANA and PLAXIS. However, after the phase transformation, the sand acquires an expansive behavior, which is modeled differently in the two programs. This does not indicate an incorrect model implementation, but may be due to various factors, such as differences in the analysis capability between the two programs. However, from an engineering perspective, both curves represent the same phenomenon.

In undrained conditions, the application of load leads to increases in pore water pressure. Following the literature review and based on the contributions of [16, 34], the main input parameters that influence the simulation of the triaxial compression test in tailings sands were estimated for use in the UBCSAND model [22]. These parameters were determined under an isolation constraint of 5 kg/cm^2. Initially, the reference pressure P_{ref}, was established based on values from previous studies. For the present analysis, it was set at 100 kPa.

TABLE I. PARAMETERS THAT HAVE A MAJOR IMPACT ON THE MODELING OF TRIAXIAL COMPRESSION TESTING

Parameters	UBCS and PLAXIS dilating	UBCS and PLAXIS contractive	UBCS and PLAXIS very contractive	UBCS and TNO Diana dilating	UBCS and TNO Diana contractive	UBCS and TNO Diana very contractive
K_B^e	400	600	600	400	600	600
K_G^e	900	400	400	900	400	400
K_G^p	400	800	800	400	800	800
n_e	0.5	0.5	0.5	0.5	0.5	0.5
m_e	0.5	0.5	0.5	0.5	0.5	0.5
n_p	0.5	0.5	0.5	0.5	0.5	0.5
ϕ_{cv}	32°	32°	32°	32°	32°	32°
ϕ_{peak}	33°	32°	31°	33°	32°	31°
c	0	0	0	0	0	0
R_f	0.98	0.98	0.98	0.98	0.98	0.98
σ_t	100	100	100	100	100	100

IV. VALIDATION OF THE UBCSAND MODEL

The validity of the UBCSAND model was supported by the study conducted in [22], where the shear stress–shear strain and shear stress–vertical effective stress were analyzed, as displayed in Figure 3. The model demonstrated its ability to accurately replicate both the banana and the butterfly loop. This performance was attributed to the model's consideration of stress ratio history, incorporating the effect of load reversal on the plastic shear modulus. In addition, the model managed to represent the shear strain accumulation during cyclic loading in an acceptable manner.

Further validation was provided in [29], where favorable results were obtained using drained cyclic and monotonic triaxial compression tests on four different types of aggregates (gabbro, limestone, demolished concrete, and steel slag). From the analysis, the applicability of the UBCSAND model was assessed for the simulation of relevant nonlinear stress-strain curves. The parameters with the greatest impact on the simulation of the triaxial compression tests were established considering the factors identified in [34], as detailed in Table II.

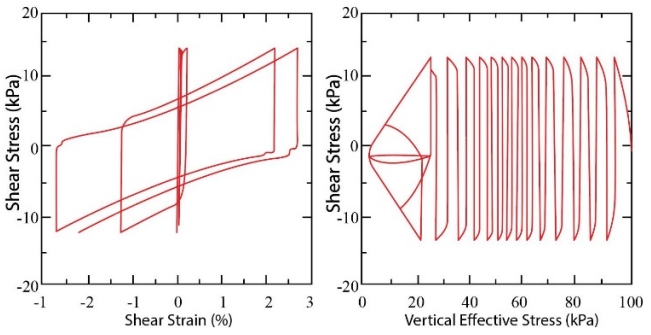

Fig. 3. Undrained cyclic DSS load response for $(N_1)_{60cs}$ = 10 of the JRA96 procedure with vertical effective consolidation stress σ_{vc0} = 101 kPa and initial static shear stress = 0.

TABLE II. KEY PARAMETERS ON THE MODELING OF TRIAXIAL COMPRESSION TESTING

Parameter	Symbol
Number of the elastic volumetric modulus	K_B^e
Plastic cutting module number	K_G^p
Angle of friction at failure	ϕ_f
Angle of friction at constant volume	ϕ_{cv}
Volumetric modulus of the fluid	K_f

Considering the default input parameters to/in the TNO DIANA software, Table III presents the values used for the validation of the UBCSAND model. For greater analysis, the results of the simulation carried out in the TNO DIANA program were presented, along with the values obtained in the simulation with the PRAXIS program. These results were then compared jointly with those obtained from the experimental tests. Figure 4 presents the behavior of the stress-strain diagram.

The results outlined in Figure 3 confirmed that, in general terms, the UBCSAND model is highly proposed for numerical simulation, since it provides reasonable and reliable results. Subsequently, numerical modeling is carried out in TNO DIANA, which implements the UBCSAND model.

TABLE III. UBCSAND MODEL ADAPTED PARAMETERS

Symbol	Description	Method	Default
P_{ref}	Reference pressure (kPa)	Curve fitting	100
m_e	Exponent of the elastic bulk modulus	Curve fitting	0.5
n_e	Exponent of the elastic shear modulus	Curve fitting	0.5
v	Poisson's ratio	-	-
K_B^e	Bulk modulus number	Triaxial test (CID or CIU)	-
K_G^e	Shear modulus number	Curve fitting	-
ϕ_0	Bulk modulus number	Triaxial test (CID or CIU)	-
n_p	Shear modulus number	Curve fitting	-
K_G^p	Initial friction angle (°)	Triaxial test (CID or CIU)	0°
ϕ_f	Plastic shear modulus exponent	Curve fitting	0.5
R_f	Plastic shear modulus number	Curve fitting	-
ϕ_{cv}	Friction angle at failure (°)	Triaxial test (CID or CIU)	-
Δ_p	Failure ratio	Curve fitting	0.9
P_t	Constant volume friction angle (°)	Triaxial test (CID or CIU)	-
n	Pressure change (kPa)	Triaxial test (CID or CIU)	0
B_{skem}	Tensile parameter (kPa)	Curve fitting	0
K_f	Porosity	Volumetric relationships	-
f_{acpre}	Skempton's B parameter	Triaxial test (CID or CIU)	-
f_{acpost}	Fluid bulk modulus (kPa)	Curve fitting	-

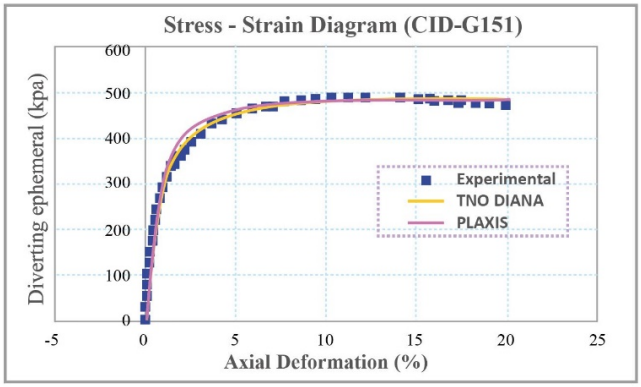

Fig. 4. Undrained monotonic response of samples of *Dr* = 40 %, axial pore pressure-strain curves for different confining pressures.

A. Experimental Response

The process began with the preparation and testing of tailings sand samples, at confining pressures of 5, 10, and 15 kg/cm^2 with a relative density of 40%. Controlled deformation conditions were performed at a strain rate of 0.13 mm/min. For all tests, double membranes were applied, and the back pressure was 4 and 5 kg/cm^2 in order to avoid cavitation.

Following that, the UBCSAND model parameters were calculated for a confining stress of 5 kg/cm^2. These values were

then incorporated into the numerical model in TNO DIANA, which defines the type of test, the generation of the model, and the application of loads. The tailings sands used in this study contained a fine content of 23% and is classified as silty sand according to ASTM D4318. The maximum and minimum densities were determined using the Japanese method (JSSMFE) for the maximum and the slow sedimentation of the dry material within a mold of known dimensions for the minimum density (ASTM D4254). Table IV presents the characteristics of the tailings sands.

TABLE IV. TAILINGS SAND CHARACTERISTICS

Characteristics		Unit	Value
Specific gravity		g/cm^3	2.77
USCS classification		N/A	SM
Maximum void ratio	max	-	1.111
Minimum void ratio	min	-	0.462

The tailings sand specimens were prepared using the Moist Tamping wet compaction method. Cylindrical specimens with a diameter of 5 cm and a height of 10 cm were made within triaxial cells and wrapped with a latex membrane. Then, the specimens were mounted in the triaxial apparatus, and the sample was saturated filling all the interstices of the specimen. Once saturated, the specimens underwent isotropic consolidation before being sheared to failure under controlled conditions. The chamber pressures, back pressures, and effective chamber pressures at which the specimens were tested are presented in Table V.

TABLE V. PRESSURE APPLIED TO STATIC TRIAXIAL TESTS

Chamber pressure, σ_0 (kg/cm^2)	Back pressure (kg/cm^2)	Effective chamber pressure, σ'_0 (kg/cm^2)
10.0	5.0	5.0
14.0	4.0	10.0
19.0	4.0	15.0

The results of the static triaxial tests performed in the undrained condition and the final void ratio obtained after consolidation are shown in Table VI. From these values, the ultimate state line and the isotropic consolidation curve in the e-log (p') plane can be obtained.

TABLE VI. RESULTS OF STATIC TRIAXIAL TESTS

Effective chamber pressure, σ_0 (kg/cm^2)	Void ratio (e)	q' (kg/cm^2)	p' (kg/cm^2)
5.0	0.779	2.25	2.57
10.0	0.766	4.11	4.95
15.0	0.716	5.61	6.97

B. Experimental Behavior

Figures 5-7 depict the experimental responses of the undrained behavior of tailings sands for a density of 40% and confining pressures of 5, 10, and 15 kg/cm^2. In Figure 5, it is obvious that in the stress-strain curves, there is a continuous growth of the resistance to the increase in axial strain. For all test cases, a stabilization of the deviatoric stress is observed from 15% strain onwards.

In Figure 7, it can be seen that the Critical State Line (CSL) is well defined with the stress level reached. The critical state angle is 40.6°.

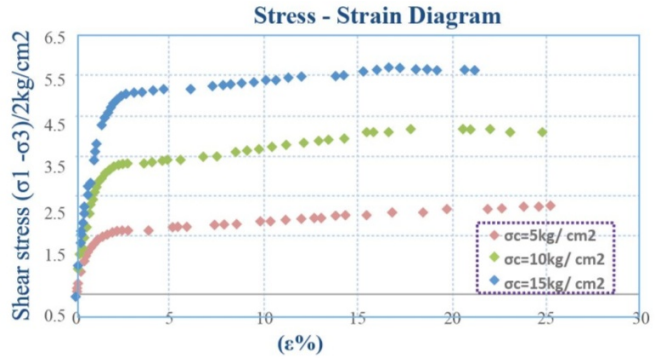

Fig. 5. Undrained monotonic response of samples of Dr = 40%, axial stress-strain curves for different confining pressures.

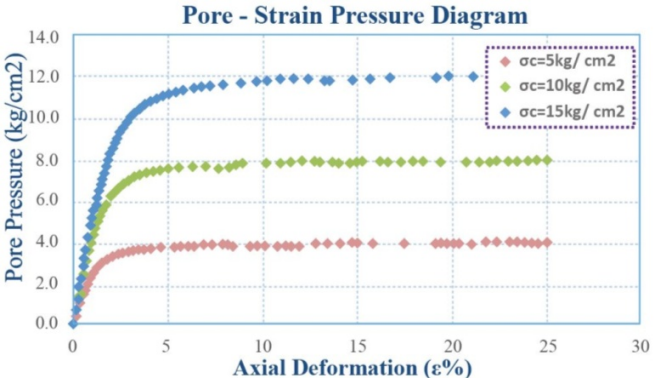

Fig. 6. Undrained monotonic response of samples of Dr = 40%, axial pore pressure-strain curves for different confining pressures.

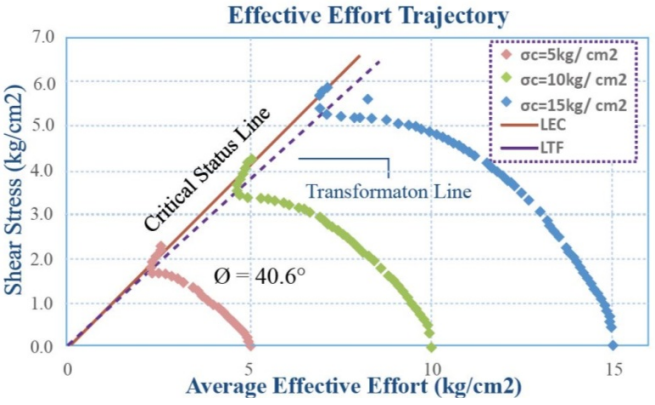

Fig. 7. Undrained monotonic response of samples of Dr = 40%, effective stress path for different confining pressures

C. Numerical Modeling

The numerical analysis began with the calculation of the model parameters, previously discussed. Then, the sand was modeled in the TNO Diana program, where the results were generated with the application of load, specified according to the contributions of [22, 30] for the validation of the

UBCSAND model. Table VII summarizes the formulas and criteria used in the model calibration, while Table VIII presents the calibrated parameters of the UBCSAND model for all studied sand samples. These parameters for the monotonic triaxial test were calculated as 5 kg/cm^2. The calculation of the parameters for the confinement tests of 10 and 15 kg/cm^2 followed the same line.

TABLE VII. FORMULAS AND CRITERIA USED IN THE CALIBRATION OF THE UBCSAND MODEL

Symbol	Description	Criteria or formula	Observation
P_{ref}	Reference pressure	$P_{ref} = 100\ kPa$	Atmospheric pressure
m_e	Exponent of the volumetric elastic modulus	$m_e = 0.50$*	-
n_e	Exponent of the elastic shear modulus	$n_e = 0.50$*	-
v	Poisson's ratio	$v = \frac{E}{2G} - 1$	E:Coefficient of elasticity or Young's modulus, G: modulus of rigidity
K_B^e	Number of the elastic volumetric modulus	$K_B^e = \frac{2V_0}{(V_0 - V_f)} (\frac{p}{P_{ref}})^{0.5}$	-
K_G^e	Elastic shear modulus number	$\frac{K_G^e}{K_B^e} = \frac{3(1-2v)}{2(1+v)}$	-
ϕ_0	Initial friction angle	ϕ_0	$\phi_{0=0}$
n_p	Plastic shear modulus exponent	n_p* = 0.50	-
K_G^p	Plastic cutting modulus number	$G_s^p = K_G^p (\frac{p}{P_{ref}})^{np-1}$	-
ϕ_f	The angle of friction at failure	$M = \frac{6\sin(\varphi_f)}{3 - \sin(\varphi_f)}$	-
R_f	Failure ratio	$R_f = \frac{\eta_f}{\eta_{ult}}$	-
ϕ_{cv}	The angle of friction at constant volume	$\sin(\phi_{cv}) = 0.64$	-
Δ_p	Pressure change	$\Delta_p = 0$	-
P_t	Tensile parameter	$P_t = 0$	-
n	Porosity	$n = \frac{e}{1+e}$, $e = 0.779$	e: Vacuum index
B_{skem}	Skempton Parameter B	$B_{skem} = 0.99$	-
K_f	Volumetric modulus of the fluid	$K_f = \frac{nK^e}{\frac{1}{B_{Skem}-1}}$	$K^e = K_B^e P_{ref}$
f_{acpre}	Pre liquefaction factor	$f_{acpre} = 1$	-
f_{acpost}	Post liquefaction factor	$f_{acpost} = 1$	-

Consequently, these values were incorporated into the finite element program TNO DIANA, which graphically represents the corresponding relationships, as illustrated in Figures 8-16. In Figures 8-10, the UBCSAND model exhibited an acceptable performance with respect to the experimental data (i.e., it effectively denoted the elastic and plastic sand behavior.) It also indicated a contractive behavior and consequently a dilatant performance in the transformation phase, where it detected approximately a shear stress of 1.7 kg/cm^2.

TABLE VIII. CALIBRATED PARAMETERS OF THE UBCSAND MODEL FOR ALL STUDIED SAND SAMPLES

Symbol	Description	σ_c (kg/cm$_2$)		
		5	10	15
P_{ref}	Reference pressure	100 kPa	100 kPa	100 kPa
m_e	Exponent of the volumetric elastic modulus	0.5	0.5	0.5
n_e	Exponent of the elastic shear modulus	0.5	0.5	0.5
v	Poisson's ratio	0.125	0.125	0.125
K_B^e	Number of the elastic volumetric modulus	100	100	100
K_G^e	Elastic shear modulus number	100	100	100
ϕ_0	Initial friction angle	0°	0°	0°
n_p	Plastic shear modulus exponent	0.5	0.5	0.5
K_G^p	Plastic cutting module number	77.5	77.5	77.5
ϕ_f	The angle of friction at failure	40.6°	40.6°	40.6°
R_f	Failure ratio	0.85	0.85	0.85
ϕ_{cv}	The angle of friction at constant volume	40°	40°	40°
Δ_p	Pressure change	0 kPa	0 kPa	0 kPa
P_t	Tensile parameter	0 kPa	0 kPa	0 kPa
n	Porosity	0.438	0.434	0.417
B_{skem}	Skempton Parameter B	0.99	0.95	0.95
K_f	Volumetric modulus of the fluid	433,507 kPa	82,412 kPa	79,277 kPa
f_{acpre}	Pre liquefaction factor	1	1	1
f_{acpost}	Post liquefaction factor	1	1	1

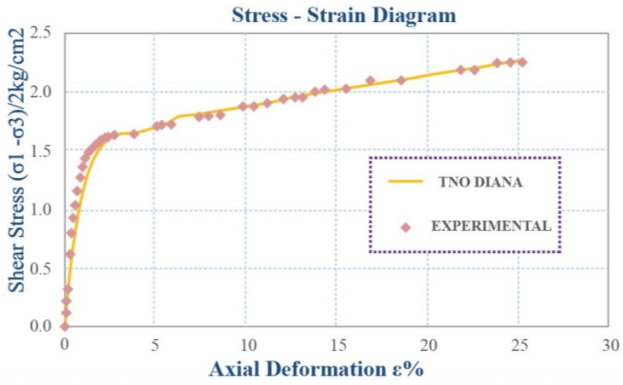

Fig. 8. Undrained stress-strain behavior with a relative density of 40% and confining stress of σ'_0 = 5 kg/cm^2.

Figures 11-13 further illustrate that even though the UBCSAND model is complex, it enables complementing the traditional empirical methods for characterizing the sand behavior. Once again, the model shows high accuracy during the transformation phase with a shear stress of approximately 3.5 kg/cm^2. The results presented in Figures 14-16 confirm that the model effectively represents the elastoplastic behavior of the sand. In this sense, the parameters used in the modeling result from a calibration adjusted to the needs of the study. Under a confining stress of σ'_0 = 15 kg/cm^2, the shear stress was approximately equal to 5.5 kg/cm^2. Finally, for tailings sands with a relative density of 40%, the CSL was found at an angle of 40.6°, while the phase transformation line was positioned at an angle of approximately 38°.

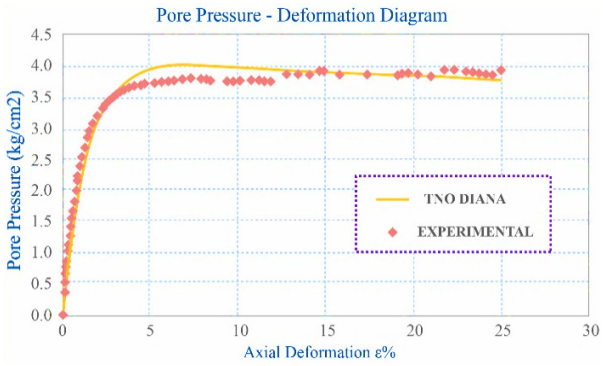

Fig. 9. Pore-strain variation behavior of sand for a relative density of 40% and confining stress of σ'_0= 5 kg/cm^2.

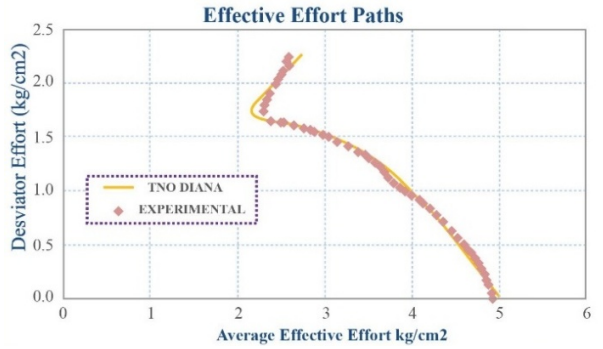

Fig. 10. Stress path behavior of sand for a relative density of 40% and confining stress of σ'_0= 5 kg/cm^2.

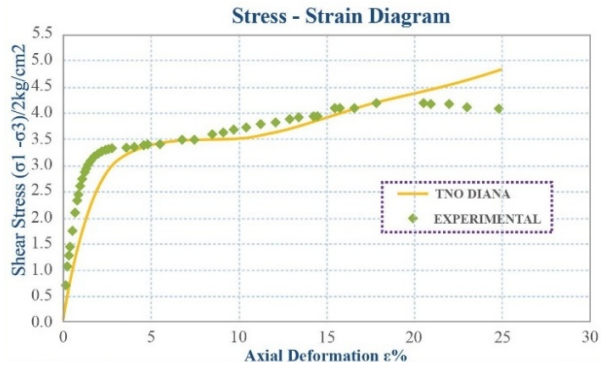

Fig. 11. Behavior according to undrained stress-strain, with a relative density of 40% and confining stress of σ'_0= 10 kg/cm^2.

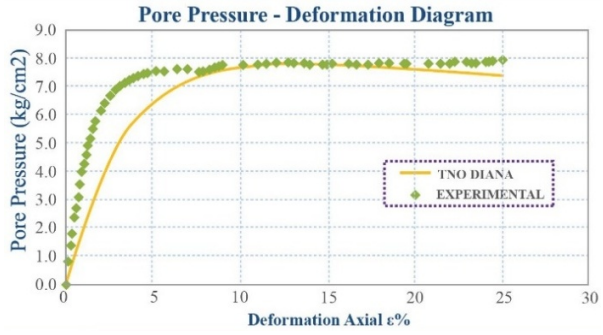

Fig. 12. Pore-strain variation behavior of sand for a relative density of 40% and confining stress of σ'_0 = 10 kg/cm^2.

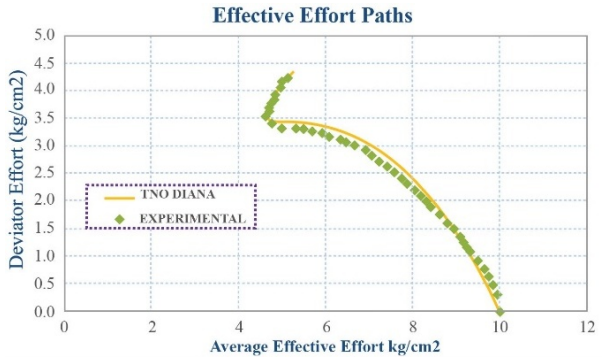

Fig. 13. Stress path behavior of sand for a relative density of 40% and confining stress of σ'_0 = 10 kg/cm^2.

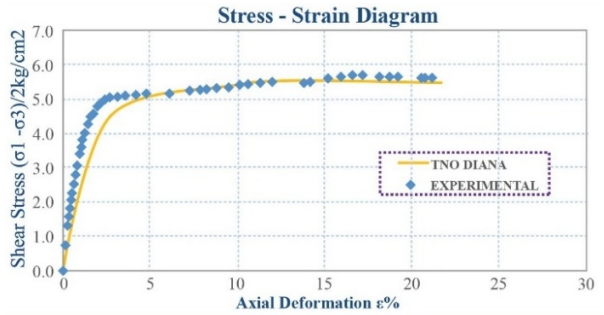

Fig. 14. Behavior according to undrained stress-strain, with a relative density of 40% and confining stress of σ'_0 = 15 kg/cm^2.

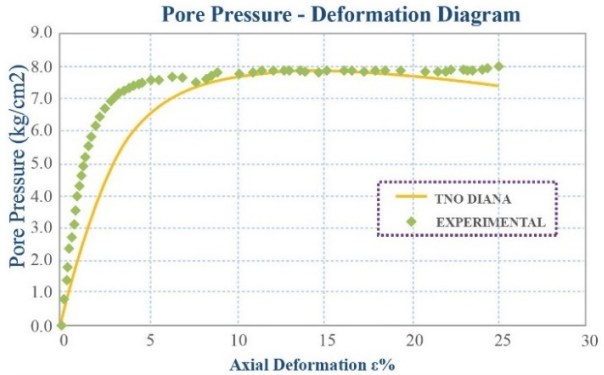

Fig. 15. Pore-strain variation behavior of sand for a relative density of 40% and confining stress of σ'_0 = 15k g/cm^2.

Fig. 16. Stress path behavior of sand for a relative density of 40% and confining stress of σ'_0 = 15 kg/cm^2.

V. DISCUSSION

The mechanical behavior of tailings sands was simulated with high accuracy through the use of the UBCSAND constitutive model with a numerical analysis, following methodologies from previous studies [22, 29]. The numerical response of the stress-strain, volumetric change-strain, and stress path exhibited a strong correlation with the experimental data obtained from triaxial tests after a successful calibration, especially at a confining stress of 5 kg/m^2, as described in [29]. This correlates with the procedures performed and results obtained in [28], where it was possible to verify the existence of an excellent agreement between the experiment and numerical calculation. Subsequently, this modeling was used to numerically simulate a driven pile installation, where the results of both were compared with the recorded experimental data, confirming a behavior of high similarity.

Under higher confinement levels, 10 and 15 kg/m^2, the model generated an acceptable to moderate approximation, due to the complex characteristics of the sand and its elastoplastic behavior, (i.e., the higher the applied load was, the greater was its deformation.) The results align with those of [7], where the mechanical properties of tailings sands saturated with different particle sizes were studied. It was observed that the larger the particle size is, the higher the shear strength will be. Regarding the findings of [30], a methodology very similar to the present one was utilized, particularly in the simulation of liquefaction scenarios. The results obtained by the UCBSAND 2 model demonstrated that the development of the fault shear band on the upstream side was consistent with the post-liquefaction slip analysis. However, the positive and beneficial findings in predicting behavior through numerical analysis remained highly effective with the use of the UCBSAND model in both versions.

Finally, the results validate the versatility of the UBCSAND constitutive model, indicating that it is a viable option for future similar investigations, including the numerical analysis of the mechanical behavior in conventional sand. As in [16], where satisfactory results were obtained with the Modified Cam-Clay and NorSand models, the UBCSAND model could be considered for future research in similar contexts.

VI. CONCLUSION

This investigation studied the application of the UBCSAND constitutive model in simulating the mechanical behavior of tailing sand through numerical analysis. The performance of the model was validated by comparing simulated results with experimental data from undrained triaxial tests under different confining pressures to ascertain the reliability of the model in replicating key aspects of shear strength, volumetric response, and phase transformation under varying loading conditions.

The following conclusions are drawn:

- From the stress-strain, pore pressure-strain, and effective stress path curves, it can be seen that the UBCSAND constitutive model implemented in TNO DIANA exhibits a significant approach to the mechanical behavior of the 40% density sand under study.
- At 5 kg/m^2 confining stress, the UBCSAND model exhibited similar response trends with that of experimental data.
- When increasing confining stress to 10 kg/m^2 and 15 kg/m^2, the model maintained quite well in general trends of soil behavior, with some moderate observations, especially under undrained conditions.
- Downslope phase transformation during undrained loading was observed for all samples with 40% relative density. Contractive behavior and excess pore pressure build-up were well simulated, which further led to effective stress reduction, a behavior associated with loose or silty sand nearing liquefaction.

Finally, it can be pointed out that the UBCSAND model in the execution of the numerical analysis of tailings sands facilitates a detailed reasoning of the behavior under different loading conditions. In that sense, it is possible to obtain insights or deductions about shear strength, the influence of relative density, and confinement. These elements are crucial for the design and evaluation of geotechnical structures where tailings sands represent a significant mechanism, in scenarios such as tailings dams or foundations in mining areas.

REFERENCES

[1] Y. Wang *et al.*, "Identification study of soil types based on feature factors of XRF spectrum combining with machine learning," *Spectrochimica Acta Part B: Atomic Spectroscopy*, vol. 219, Sep. 2024, Art. no. 107001, https://doi.org/10.1016/j.sab.2024.107001.

[2] C. E. Augarde, S. J. Lee, and D. Loukidis, "Numerical modelling of large deformation problems in geotechnical engineering: A state-of-the-art review," *Soils and Foundations*, vol. 61, no. 6, pp. 1718–1735, Dec. 2021, https://doi.org/10.1016/j.sandf.2021.08.007.

[3] L. Perkins, A. C. D. Royal, I. Jefferson, and C. D. Hills, "The Use of Recycled and Secondary Aggregates to Achieve a Circular Economy within Geotechnical Engineering," *Geotechnics*, vol. 1, no. 2, pp. 416–438, Dec. 2021, https://doi.org/10.3390/geotechnics1020020.

[4] N. Ecemis, "Experimental and numerical modeling on the liquefaction potential and ground settlement of silt-interlayered stratified sands," *Soil Dynamics and Earthquake Engineering*, vol. 144, May 2021, Art. no. 106691, https://doi.org/10.1016/j.soildyn.2021.106691.

[5] C. Monje, G. Suazo, C. Monje, and G. Suazo, "Drained cyclic behavior and minimum payback design in tailings dams," *Obras y proyectos*, no. 25, pp. 30–34, 2019, https://doi.org/10.4067/S0718-28132019000100030.

[6] G. Bella and G. Musso, "Liquefaction susceptibility of silty tailings under monotonic triaxial tests in nearly saturated conditions," *Geomechanics and Engineering, An Int'l Journal*, vol. 36, no. 3, pp. 247–258, 2024.

[7] X. Chai, Y. Sheng, J. Liu, Y. Xu, and H. Liu, "Experimental Study on the Mechanical Properties of Saturated Tailing Sand with Different Particle Sizes," *Applied Sciences*, vol. 12, no. 23, Jan. 2022, Art. no. 12231, https://doi.org/10.3390/app122312231.

[8] D. Zhang, X. Zhang, and W. Du, "DEM-FEM based numerical analysis on mechanical responses of sandy soil and pipeline to seepage erosion," *Engineering Geology*, vol. 310, Dec. 2022, Art. no. 106868, https://doi.org/10.1016/j.enggeo.2022.106868.

[9] B. J. Shwan, "Numerical analysis of slopes treated by nano-materials," *Journal of the Mechanical Behavior of Materials*, vol. 32, no. 1, Jan. 2023, https://doi.org/10.1515/jmbm-2022-0227.

[10] J. G. Liu, B. Xu, L. Sun, B. Li, and G. J. Wei, "In situ stress field in the Athabasca oil sands deposits: Field measurement, stress-field modeling, and engineering implications," *Journal of Petroleum Science and Engineering*, vol. 215, Aug. 2022, Art. no. 110671, https://doi.org/10.1016/j.petrol.2022.110671.

[11] X. Ouyang, Z. Wu, B. Shan, Q. Chen, and C. Shi, "A critical review on compressive behavior and empirical constitutive models of concrete," *Construction and Building Materials*, vol. 323, Mar. 2022, Art. no. 126572, https://doi.org/10.1016/j.conbuildmat.2022.126572.

[12] M. J. R. Vargas, R. L. H. Enrique, F. J. G. Bautista, Á. B. L. Pérez, and A. C. B. Ramos, "Structural analysis of a rigid solid frame structure," *Dominio de las Ciencias*, vol. 9, no. 3, pp. 321–335, Jul. 2023, https://doi.org/10.23857/dc.v9i3.3445.

[13] V. M. Sadovskii, O. V. Sadovskaya, and I. E. Petrakov, "On the theory of constitutive equations for composites with different resistance in compression and tension," *Composite Structures*, vol. 268, Jul. 2021, Art. no. 113921, https://doi.org/10.1016/j.compstruct.2021.113921.

[14] F. dell'Isola and M. Stilz, "The «materialization» of forces: Why confounding mathematical concept and physical entity makes the design of metamaterials arduous," *ZAMM - Journal of Applied Mathematics and Mechanics*, vol. 103, no. 2, 2023, Art. no. e202200433, https://doi.org/10.1002/zamm.202200433.

[15] I. van Zelst, F. Crameri, A. E. Pusok, A. Glerum, J. Dannberg, and C. Thieulot, "101 geodynamic modelling: how to design, interpret, and communicate numerical studies of the solid Earth," *Solid Earth*, vol. 13, no. 3, pp. 583–637, Mar. 2022, https://doi.org/10.5194/se-13-583-2022.

[16] A. de O. Faria, B. G. Delgado, L. D. Ferreira, and M. P. dos Santos Junior, "Comparative evaluation of constitutive models for stress-strain analysis of an iron ore tailings from the Quadrilátero Ferrífero, Minas Gerais, Brazil," *Soils and Rocks*, vol. 47, 2023, Art. no. e2024011022.

[17] R. Kabo, M.-A. Bourgault, J. F. Bissonnette, N. Barrette, and L. Tanguay, "Use of Mixed Methods in the Science of Hydrological Extremes: What Are Their Contributions?," *Hydrology*, vol. 10, no. 6, Jun. 2023, Art. no. 130, https://doi.org/10.3390/hydrology10060130.

[18] B. Peters, B. Eddy, D. Galvin-McLaughlin, G. Betz, B. Oken, and M. Fried-Oken, "A systematic review of research on augmentative and alternative communication brain-computer interface systems for individuals with disabilities," *Frontiers in Human Neuroscience*, vol. 16, Jul. 2022, https://doi.org/10.3389/fnhum.2022.952380.

[19] A. C. Schindele and M. and Lindroth, "Sexual and reproductive health and rights (SRHR) among young people in secure state care and their non-incarcerated peers – a qualitative, descriptive and comparative study," *European Journal of Social Work*, vol. 24, no. 4, pp. 657–670, Jul. 2021, https://doi.org/10.1080/13691457.2020.1815658.

[20] R. J. Pidduck, D. M. Townsend, and L. W. Busenitz, "Non-probabilistic reasoning in navigating entrepreneurial uncertainty: A psychology of religious faith lens," *Journal of Business Venturing*, vol. 39, no. 4, Jul. 2024, Art. no. 106392, https://doi.org/10.1016/j.jbusvent.2024.106392.

[21] K. Linka, M. Hillgärtner, K. P. Abdolazizi, R. C. Aydin, M. Itskov, and C. J. Cyron, "Constitutive artificial neural networks: A fast and general approach to predictive data-driven constitutive modeling by deep learning," *Journal of Computational Physics*, vol. 429, Mar. 2021, Art. no. 110010, https://doi.org/10.1016/j.jcp.2020.110010.

[22] J.-C. Chou, H.-T. Yang, and D.-G. Lin, "Calibration of Finn Model and UBCSAND Model for Simplified Liquefaction Analysis Procedures," *Applied Sciences*, vol. 11, no. 11, Jun. 2021, Art. no. 5283, https://doi.org/10.3390/app11115283.

[23] R. Verdugo, "Static liquefaction in the context of steady state/critical state and its application in the stability of tailings dams," *Soil Dynamics and Earthquake Engineering*, vol. 176, Jan. 2024, Art. no. 108270, https://doi.org/10.1016/j.soildyn.2023.108270.

[24] F. Qamar and S. Qin, "Development of Nonlinear Finite Element Models of Mortar-Free Interlocked Single Block Column Subjected to Lateral Loading," *Arabian Journal for Science and Engineering*, vol. 46, no. 11, pp. 11047–11062, Nov. 2021, https://doi.org/10.1007/s13369-021-05668-7.

[25] L. U. Argiento, Celano ,Thomas, Ceroni ,Francesca, and C. and Casapulla, "Modelling Strategies for the In-plane Behaviour of Iron-framed Masonry Structures: Parametric Analysis on Simple Panels and a Church Façade," *International Journal of Architectural Heritage*, vol. 16, no. 7, pp. 1006–1031, Jul. 2022, https://doi.org/10.1080/15583058.2020.1858369.

[26] D. Arndt *et al.*, "The deal.II finite element library: Design, features, and insights," *Computers & Mathematics with Applications*, vol. 81, pp. 407–422, Jan. 2021, https://doi.org/10.1016/j.camwa.2020.02.022.

[27] S. Maraš-Dragojević, "Use of finite element method for 2D and 3D analyses of tunnelling induced settlements," *Građevinar*, vol. 72, no. 8, pp. 673–680, 2020, https://doi.org/10.14256/JCE.2119.2017.

[28] S. Giridharan, S. Gowda, D. F. E. Stolle, and C. Moormann, "Comparison of UBCSAND and Hypoplastic soil model predictions using the Material Point Method," *Soils and Foundations*, vol. 60, no. 4, pp. 989–1000, Aug. 2020, https://doi.org/10.1016/j.sandf.2020.06.001.

[29] E. Voyagaki, T. Kishida, R. F. Aldulaimi, and G. Mylonakis, "Integration and calibration of UBCSAND model for drained monotonic and cyclic triaxial compression of aggregates," *Soil Dynamics and Earthquake Engineering*, vol. 171, Aug. 2023, Art. no. 107978, https://doi.org/10.1016/j.soildyn.2023.107978.

[30] N.-P. Doan, B.-P. Nguyen, and S.-S. Park, "Seismic deformation analysis of earth dams subject to liquefaction using UBCSAND2 model," *Soil Dynamics and Earthquake Engineering*, vol. 172, Sep. 2023, Art. no. 108003, https://doi.org/10.1016/j.soildyn.2023.108003.

[31] S.-S. Park, "A two mobilized-plane model and its application for soil liquefaction analysis," PhD dissertation, University of British Columbia, CA, 2005.

[32] D. Figueira, C. Sousa, and A. S. Neves, "Constitutive Model for Aggregate Interlock in FEM Analyses of Concrete Interfaces with Embedded Steel Bars," *International Journal of Concrete Structures and Materials*, vol. 14, no. 1, Mar. 2020, Art. no. 15, https://doi.org/10.1186/s40069-019-0390-8.

[33] A. B. Tsegaye, "Plaxis Liquefaction Model," Delf, Netherlands, Technical Report 1, 2010.

[34] Y. Feng, "Dynamic response of tunnel through water-rich liquefiable layer based on UBC3D-PLM model," *Vibroengineering Procedia*, vol. 49, pp. 51–55, May 2023, https://doi.org/10.21595/vp.2023.23219.